Study on Electrical Machine Phase Current Reconstruction Based on a DC-bus Current Sensor

Yu-Chao Fang, Yun-Chong Wang, *Member*, *IEEE*, Zhang-Hao Huang, *Member*, *IEEE*, Yue-Sheng Qi, *Student Member*, *IEEE*, and Jian-Xin Shen, *Fellow*, *CES and Senior Member*, *IEEE*

***Abstract*—In the field of high-performance motor control, accurate sampling of motor currents is essential for precise control and stability. To achieve reliable measurement of a motor's three-phase currents, it is typically necessary to install at least two high-precision current sensors. However, using multiple sensors increases the volume and cost of the control system, thereby creating challenges for cost management and controller miniaturization. This paper investigates a phase current reconstruction technique that employs only one current sensor mounted on the direct current (DC) bus. The primary goal is to address the current reconstruction dead zones that occur in low modulation regions and sector boundary regions under space vector pulse width modulation (SVPWM) control. To resolve this issue, two hybrid pulse width modulation (HPWM) methods are proposed: one combining remote state pulse width modulation (RSPWM), near state pulse width modulation (NSPWM), and SVPWM, and the other combining RSPWM and NSPWM. Experiments with different voltage utilization have been conducted for both types of HPWM. Both schemes enable 100% voltage utilization for motor control utilizing only a DC-bus current sensor, and the algorithm for HPWM determination has been introduced..**

***Index Terms*—Direct current (DC)-bus current sensor, motor control, Near state pulse width modulation (NSPWM), Phase current reconstruction, Remote state pulse width modulation (RSPWM), Space vector pulse width modulation (SVPWM).**

I. INTRODUCTION

For high-performance three-phase electrical machine control, the dual closed-loop control scheme is commonly employed to drive machines, which has the advantages of strong anti-interference ability, fast response, and operation stability. To implement vector control, it is necessary to obtain the information of three-phase currents, which is typically achieved through the installation of three current sensors for phase current detection. However, installing multiple sensors increases the volume and cost of the control system. Therefore, some studies have proposed a current reconstruction technique based on a direct current (DC)-bus current sensor [1]. It can not only reduce the volume and cost of the whole system, but also be used as a fault-tolerant operation scheme for some high-reliability applications where phase current sensor failure might occur.

By installing a current sensor on the DC bus, different phase currents can be measured according to different switching states. In the space vector pulse width modulation (SVPWM) control method, the voltage vector within each cycle is composed of zero voltage vectors and two adjacent non-zero voltage vectors. Assuming that the phase currents remain constant during a pulse width modulation (PWM) cycle, two phase currents are measured during the application of two non-zero voltage vectors. Subsequently, the third phase current value is calculated based on the principle that the sum of the three-phase currents is zero.

The utilization of SVPWM encounters a challenge in current sampling completion due to the requisite duration of non-zero vectors. Consequently, a phase current reconstruction blind zone arises with SVPWM implementation. In the sector boundary regions, there is a non-zero voltage vector whose duration time is too short to complete the sampling, so that only one phase current can be measured. And in the low modulation region, the duration times of the two non-zero voltage vectors are too short to complete the current sampling of either phase. Therefore, there is a phase current reconstruction blind zone at both the sector boundary region and the low modulation region when employing SVPWM. In response to this challenge, various studies have explored alternative strategies. Some studies have proposed the pulse insertion method, which involves inserting three non-zero voltage vectors after each SVPWM cycle for current measurement [2]-[6]. Nevertheless, this approach incurs increased switching losses and prolongs PWM cycle with zero voltage, consequently reducing voltage utilization. Some studies proposed the pulse shift method, which trims the PWM waveform by shifting it to extend the corresponding voltage vector duration [7]-[11]. However, this method is computationally complex and difficult to realize in industrial embedded systems. Reference [12] addressed the low voltage utilization issue of the pulse shift method through the application of overmodulation control. Reference [13]

Manuscript received December 4, 2025; revised March 16, 2026; accepted April 24, 2026. Date of publication June 25, 2026. Date of current version May 21, 2026.

This work was supported by the Natural Science Foundation of China under Grant U22A20214.

Yu-Chao Fang is with Tianjin Research Institute of Electric Science Co., Ltd., Tianjin 300180, China, and also with the College of Electrical Engineering, Zhejiang University, Hangzhou 310027, China. Yun-Chong Wang, Zhang-Hao Huang, Yue-Sheng Qi, and Jian-Xin Shen are with the College of Electrical Engineering, Zhejiang University, Hangzhou 310027, China. (e-mail: ycfang95@zju.edu.cn, wangycee@zju.edu.cn, Zhanghao_H@zju.edu.cn, 22310058@zju.edu.cn, J_X_Shen@ zju.edu.cn)

(*Corresponding Author: Yun-Chong Wang*)

Digital Object Identifier 10.30941/CESTEMS.2026.00016

introduced a non-zero compensation vector PWM method. However, this method involves a phase switching four times between two sectors, thereby increasing switching losses. Reference [14] expanded the measurable region by integrating insertion vectors into SVPWM. This method results in intensively frequent switching in the low modulation region, leading to increased switching losses. Reference [15] expanded the measurable region by using active zero state pulse width modulation (AZSPWM). Another avenue of investigation involves assuming sinusoidal phase currents when insufficient sampling time precludes accurate reconstruction. This approach utilizes observers and sinusoidal curve fitting for phase current reconstruction. However, its effectiveness relies on the validity of the sinusoidal assumption [16]-[17]. Some studies have proposed methods employing current state observers for three-phase current estimation. However, the complexity of the state observer's control structure and its sensitivity to variations in system parameter models pose significant challenges for practical implementation [18]-[20].

This paper analyzes the performance of SVPWM, remote state pulse width modulation (RSPWM), and near state pulse width modulation (NSPWM) under a DC-bus single current sensor setup. RSPWM allows phase current reconstruction without measurement blind zones in the low modulation region. NSPWM achieves the same across most of the high modulation region, except near the six corners of the voltage hexagon. To overcome the blind zones of SVPWM in both low and high modulation regions, a hybrid PWM (HPWM) method, named HPWM1, is developed that combines RSPWM, NSPWM, and SVPWM. Additionally, a simplified method using only RSPWM and NSPWM, called HPWM2, is proposed. HPWM2 also achieves nearly no phase current reconstruction blind zone across a high voltage utilization range, except at the hexagon corners. Both methods aim to minimize reconstruction blind zones and improve voltage utilization. The harmonic performance, reconstruction accuary, common-mode voltage (CMV), and switching losses of the two strategies are compared in this study. As for the medium modulation regions, HPWM1 features a lower reconstruction error; however, HPWM1 introduces higher harmonic distortion compared to HPWM2. HPWM2 achieves both lower common-mode interference and lower switching losses in medium and high modulation regions.

II. Principle of Phase Current Reconstruction

The typical voltage-source inverter configuration is shown in Fig. 1. In a three-phase inverter, there are two switching states of each phase; $S_x = 1$ (where x represents phases A, B or C) represents that the upper bridge arm of the respective phase is active. Conversely, $S_x = 0$ represents that the lower bridge arm is active. This results in a total of eight distinct switching states for inverter. The relationship between switching states and the basic voltage vectors is illustrated in Fig. 2.

PWM techniques are widely used in inverters to synthesize a continuous reference voltage by adjusting the pulse widths within each switching cycle. The resulting CMV is defined as

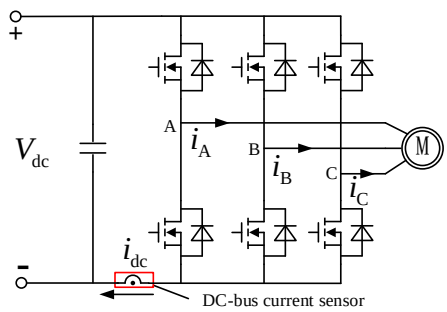

Fig. 1. Three-phase voltage source inverter with DC-bus current sensor.

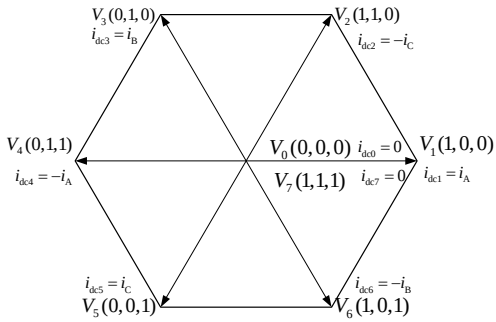

Fig. 2. DC-bus current corresponding to different voltage vectors.

$$V_{cm} = \frac{V_a + V_b + V_c}{3} \tag{1}$$

where V_a, V_b, and V_c represent the three-phase voltages [21].

The current measurement method using only one DC-bus current sensor is based on the fact that there is a correspondence between DC-bus current and phase current across varying switching states. This correspondence enables the derivation of distinct phase current information for each state of the power device's switching. The relationship between DC-bus current and phase current across different fundamental voltage vectors $V_i(S_A, S_B, S_C)$ is also illustrated in Fig. 2.

In the SVPWM control method, the voltage vector in each cycle is composed of a combination of zero voltage vectors and two adjacent non-zero voltage vectors. As shown in Fig. 3, the DC-bus current varies with the switching state corresponding to sector I in Fig. 2. During the application of V_1 and V_2, the DC-bus current is sampled to obtain the A-phase and C-phase currents, respectively. Using the principle that the sum of three-phase currents is zero, the information of all three-phase currents can be reconstructed.

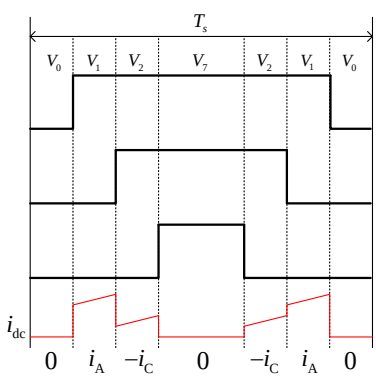

Fig. 3. The ideal waveform of DC-bus current variation with switching states.

Ideally, the current changes are synchronized with the switching state and can be sampled instantaneously. However, as illustrated in Fig. 4, discrepancies exist between the ideal and actual scenarios: The ideal current is represented by the red solid line, whereas the actual current is depicted by the black dashed line. The presence of dead time T_d is crucial to prevent simultaneous conduction in the upper and lower power devices. Additionally, factors such as switching time T_{on}, settling time T_{set} influenced by switching parameters and motor inductance, and analog-to-digital (A/D) conversion time T_{AD} further complicate the measurement process. To accurately measure the corresponding current, the activation of the voltage vector is imperative. This process necessitates a minimum duration time for the voltage vector action, which must be sufficient to capture the requisite current data effectively. This requirement is quantified in (2)

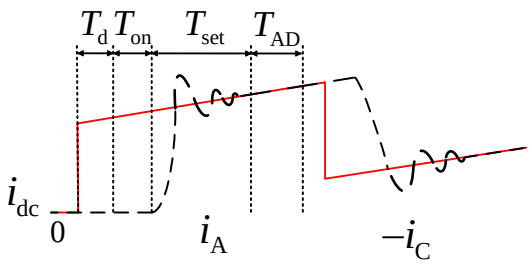

Fig. 4. Comparison of ideal current and actual current.

$$T_{min} = T_d + T_{on} + T_{set} + T_{AD} = DT_s \tag{2}$$

where T_s denotes the inverter's switching period, while D represents the ratio of the minimum duration time required for the voltage vector to the switching period.

In SVPWM, there exists a non-zero voltage vector with too short duration time for successful measurement in the sector boundary region. And in the low modulation region, both non-zero voltage vectors exhibit such a short duration time that no current information can be accurately captured for any phase. As illustrated in Fig. 5, the central hexagram region is the phase current reconstruction blind zone I in the low modulation region, where no phase current information can be obtained. The orange region is the phase current reconstruction blind zone II in the sector boundary region, where only one phase current can be obtained. And the other region is the measurable region where all three-phase currents can be reconstructed. Analytically, a region is considered measurable if at least two phase currents can be successfully sampled from the DC-bus current sampling within a PWM cycle. Conversely, a reconstruction blind zone is defined as an operating condition where only one phase current or no phase current at all can be successfully sampled. Under SVPWM, unavoidable theoretical blind zones exist in the low modulation region and at the sector's boundary region between adjacent voltage sectors.

If the four-segment SVPWM is used, where one switching period is divided into four segments instead of seven, the reconstruction blind zone is halved because the effective voltage vector is not split into two halves. However, the reconstruction blind zone is not completely eliminated.

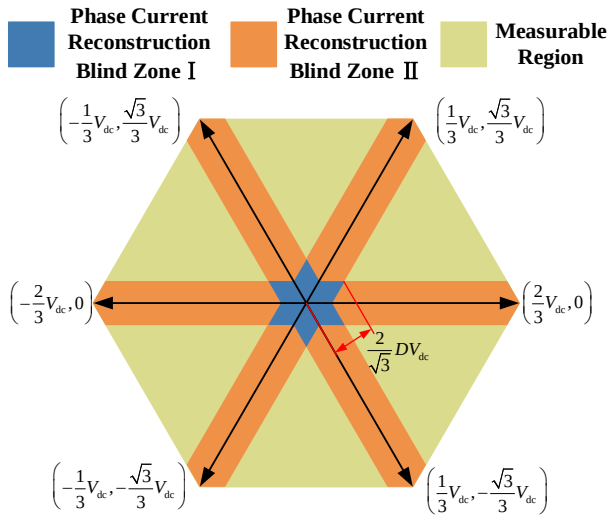

Fig. 5. Blind zone of phase current reconstruction with SVPWM. No phase current can be obtained in phase current reconstruction blind zone I, and only one phase current can be obtained in blind zone II.

III. PWM Method Based on DC-bus Current Sensor

A. *Remote State Pulse Width Modulation*

The phase current can only be obtained by sampling the DC-bus current during the application of non-zero vectors. Therefore, it is possible to synthesize the desired voltage by applying only non-zero voltage vectors within a single switching period. The desired voltage can be synthesized using three remote non-zero fundamental voltage vectors, such as V_1, V_3, and V_5, as depicted in Fig. 6. It can be seen that the CMV is constant at $\pm V_{dc}/6$. This method is known as RSPWM.

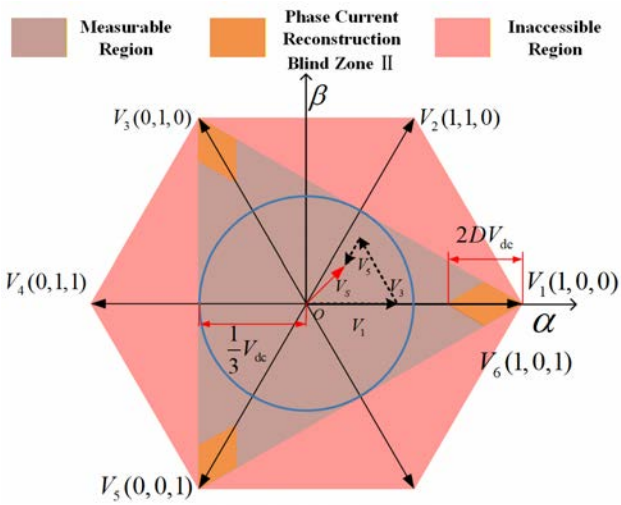

Fig. 6. Working principle of RSPWM.

According to the operational principle of RSPWM, the relationship between the specified voltage and the three effective voltage vectors within the αβ stationary reference frame satisfies (3), which can be expanded to obtain (4)

$$\begin{cases} T_s \cdot V_s = T_1 \cdot V_1 + T_3 \cdot V_3 + T_5 \cdot V_5 \\ T_s = T_1 + T_3 + T_5 \end{cases} \tag{3}$$

$$\begin{cases} T_s \cdot \begin{bmatrix} V_\alpha \\ V_\beta \end{bmatrix} = T_1 \cdot \begin{bmatrix} \frac{2}{3}V_{dc} \\ 0 \end{bmatrix} + T_3 \cdot \begin{bmatrix} -\frac{1}{3}V_{dc} \\ \frac{\sqrt{3}}{3}V_{dc} \end{bmatrix} + T_5 \cdot \begin{bmatrix} -\frac{1}{3}V_{dc} \\ -\frac{\sqrt{3}}{3}V_{dc} \end{bmatrix} \\ T_s = T_1 + T_3 + T_5 \end{cases} \tag{4}$$

where $V_{\alpha,\beta}$ denotes the voltage in the αβ phase; V_{dc} represents the DC bus voltage; T_1, T_3, and T_5 are the duration time of V_1, V_3, and V_5, respectively. The solution to these relationships yields the duration time of the three vectors as expressed in (5):

$$\begin{cases} T_1 = \frac{1}{3}T_s + \frac{V_\alpha}{V_{dc}}T_s \\ T_3 = \frac{1}{3}T_s - \frac{V_\alpha}{2V_{dc}}T_s + \frac{\sqrt{3}V_\beta}{2V_{dc}}T_s \\ T_5 = \frac{1}{3}T_s - \frac{V_\alpha}{2V_{dc}}T_s - \frac{\sqrt{3}V_\beta}{2V_{dc}}T_s \end{cases} \tag{5}$$

For the successful reconstruction of three-phase currents using RSPWM, it is essential that the duration time of at least two of the three effective voltage vectors exceeds T_{min}. The operating region of the RSPWM is depicted in Fig. 6. The orange region is the phase current reconstruction blind zone II. The central triangular region is the measurable region where RSPWM can be used to reconstruct all three-phase currents. The pink region is the inaccessible region that cannot be achieved using only the three basic voltage vectors V_1, V_3, and V_5.

Voltage utilization ratio is defined as the ratio of the maximum fundamental phase voltage an inverter can output to $V_{dc}/\sqrt{3}$. When the ratio equals unity, the applied voltage vector corresponds to the inscribed circle of the hexagon formed by the voltage vectors in the space vector diagram. The maximum amplitude of the voltage vector that can be synthesized is limited to $V_{dc}/3$ without overmodulation by V_1, V_3, and V_5. As shown in Fig. 6, the voltage utilization ratio achieved under this specific PWM control strategy is $\sqrt{3}/3$. By incorporating the basic vectors V_2, V_4, and V_6, the operational area forms a hexagram-shaped region, as illustrated by Fig. 7. As shown in Fig. 7, the maximum voltage amplitude is increased from $V_{dc}/3$ in Fig. 6 to $2\sqrt{3}V_{dc}/9$, and the voltage utilization ratio rises from $\sqrt{3}/3$ to 2/3. The CMV is constant at $\pm V_{dc}/6$ per PWM period and varies six times over each fundamental electrical cycle. This configuration covers the entire low modulation region and the sector boundary region in the medium modulation region, with reconstruction blind zones occurring only at the six corners.

B. NSPWM

NSPWM uses three near non-zero fundamental voltage vectors, such as V_6, V_1, and V_2, to synthesize the desired voltage vector, as shown in Fig. 8. It can be seen that the switching losses are reduced because one phase leg does not switch during each PWM period. Concurrently, the CMV remains at $\pm V_{dc}/6$, which varies twice within each PWM period.

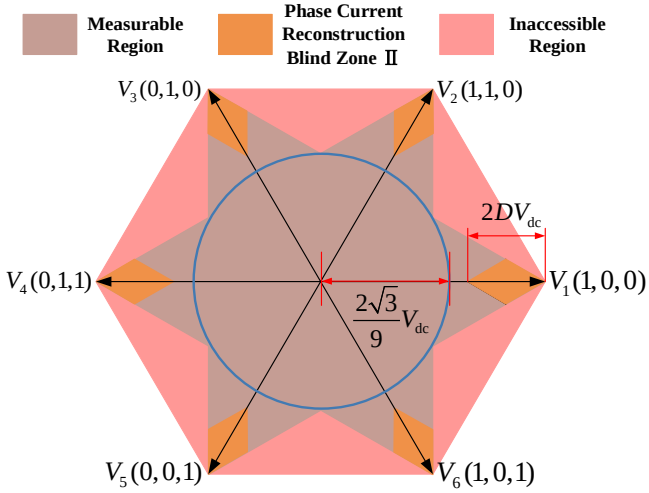

Fig. 7. Working zone of RSPWM.

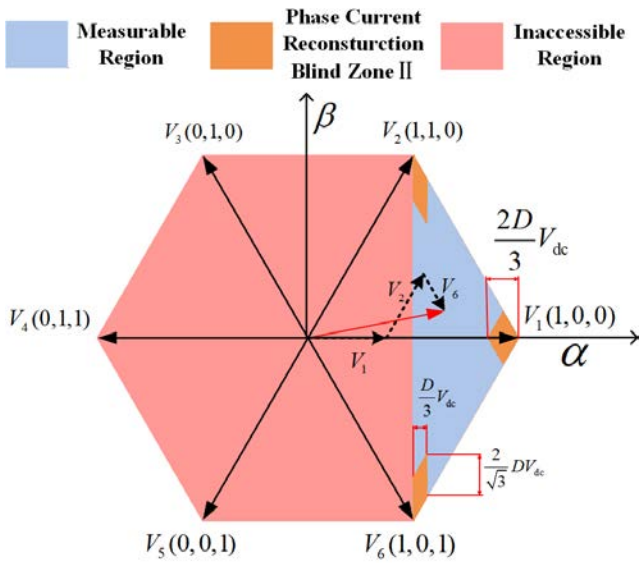

Fig. 8. Working principle of NSPWM.

Taking Fig. 8 as an example, the operational principles of NSPWM dictate that the relationship between the given voltage and the three effective voltage vectors in the αβ stationary reference frame must satisfy (6):

$$\begin{cases} T_s \cdot V_s = T_1 \cdot V_1 + T_2 \cdot V_2 + T_6 \cdot V_6 \\ T_s = T_1 + T_2 + T_6 \end{cases} \tag{6}$$

By solving (6), the duration time of these vectors is determined as follows:

$$\begin{cases} T_1 = \frac{3V_\alpha}{V_{dc}} - T_s \\ T_2 = T_s - \frac{3V_\alpha}{2V_{dc}} + \frac{\sqrt{3}V_\beta}{2V_{dc}} \\ T_6 = T_s - \frac{3V_\alpha}{2V_{dc}} - \frac{\sqrt{3}V_\beta}{2V_{dc}} \end{cases} \tag{7}$$

In order to successfully reconstruct the three-phase currents, the duration time of at least two effective voltage vectors must exceed $T_{\min}$. As a result, the effective working area in NSPWM with V_6, V_1, and V_2 is shown in Fig. 8. The entire working zone of NSPWM is shown in Fig. 9. The orange region is the phase current reconstruction blind zone II. The light blue region is the measurable region where NSPWM can be used to reconstruct all three-phase currents. The pink area is the inaccessible region that cannot be achieved.

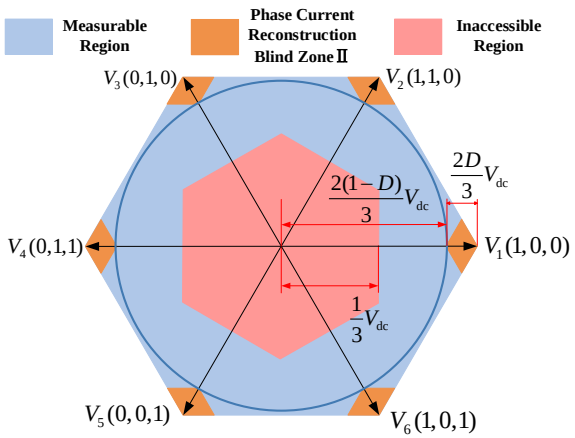

Fig. 9. Working zone of NSPWM.

C. *Hybrid Pulse Width Modulation Methods*

From the above analysis, it can be concluded that there is no reconstruction blind zone in both the low modulation region and the sector boundary region at medium modulation region with RSPWM, while there is no reconstruction blind zone in the sector boundary region at high modulation region with NSPWM. Therefore, RSPWM and NSPWM can be utilized to address the reconstruction blind zone of four-segment SVPWM in the low modulation region and sector boundary region. An HPWM that combines SVPWM with RSPWM and NSPWM, referred to as HPWM1 in this paper, has been proposed to achieve high voltage utilization without reconstruction blind zones. The operational region is illustrated in Fig. 10, RSPWM is used in the low modulation region; the combination of SVPWM with RSPWM is used in the medium modulation region, and the combination of SVPWM with NSPWM is used in the high modulation region. As shown in Fig. 10, this method can deliver a maximum fundamental phase voltage amplitude of $2(1-D)V_{dc}/3$, corresponding to a voltage utilization ratio of $2(1-D)V_{dc}/\sqrt{3}$ without current reconstruction blind zones, and achieves 100% voltage utilization when $D<1-\sqrt{3}/2$. The HPWM1 strategy ensures current continuity and control stability across its full operating range by dividing operation into specific regions. In the RSPWM and NSPWM regions, zero-voltage vectors are avoided, inherently preventing current discontinuity. In the SVPWM region, each active vector's application time exceeds $T_{\min}$, further ensuring continuity. This approach eliminates the current dropout risks inherent in conventional methods, thereby guaranteeing system controllability.

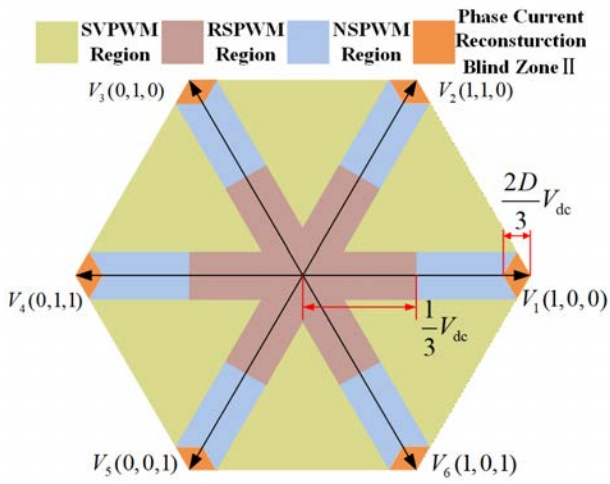

Fig. 10. Working zone of HPWM1.

As previously mentioned, NSPWM exhibits no reconstruction blind zone in the high modulation region except at the six corners of the voltage vector hexagon. However, it cannot operate in the modulation ratio region below 2/3. In contrast, RSPWM can achieve operation without reconstruction blind zone specifically within the modulation ratio region below 2/3. An HPWM that combines RSPWM with NSPWM, referred to as HPWM2 in this paper, has been proposed to achieve high voltage utilization without reconstruction blind zones. HPWM2 offers a more streamlined solution than HPWM1. It uses only two modulation strategies, while HPWM1 employs three. Despite this simplification, it maintains the same high voltage utilization and has no current reconstruction blind zones. The operational region of HPWM2 is illustrated in Fig. 11.

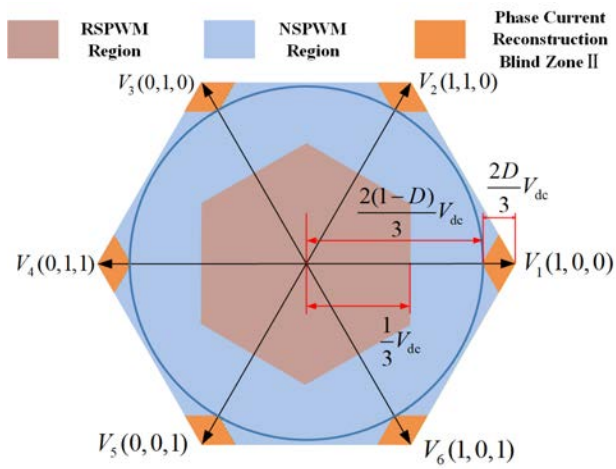

Fig. 11. Working zone of HPWM2.

It can be observed that the measurement blind zones for both HPWM schemes are confined solely to the six corners of the voltage vector hexagon. In practice, the operating voltage vector typically does not reach these extreme corners. Therefore, the reconstruction blind zones associated with the proposed HPWM controls are avoidable blind zones. Regarding CMV performance, the RSPWM scheme generates a CMV of $\pm V_{dc}/6$, which remains constant throughout a PWM period. The NSPWM scheme also produces a CMV of $\pm V_{dc}/6$,

but its polarity changes twice within one PWM period. In contrast, the SVPWM scheme yields CMV levels of $\pm V_{dc}/2$ and $\pm V_{dc}/6$, with its value changing four times per PWM period. Consequently, except in the low modulation index region where both HPWM strategies employ RSPWM and thus share identical CMV performance, HPWM2 achieves superior CMV characteristics in all other operating regions, and HPWM2 achieves superior CMV characteristics in other operating regions. Furthermore, in terms of switching losses, NSPWM maintains one phase's switching state unchanged while the other two phases switch once each per PWM period. Both RSPWM and SVPWM, however, require one switching action per phase per period. Thus, HPWM1 and HPWM2 exhibit comparable switching losses in the low modulation region, while HPWM2 achieves lower switching losses in the high modulation region.

IV. Experiment Result

In order to verify the effectiveness of the methods proposed in this paper, an experimental platform, as shown in Fig. 12, was constructed. An STM32H743 microcontroller is used in this platform to perform motor control, output PWM signals, and conduct A/D conversion operating at a switching frequency of 10 kHz. A high-frequency current probe is employed to compare the accuracy of the reconstructed current. Notably, it is not utilized as feedback for motor control.

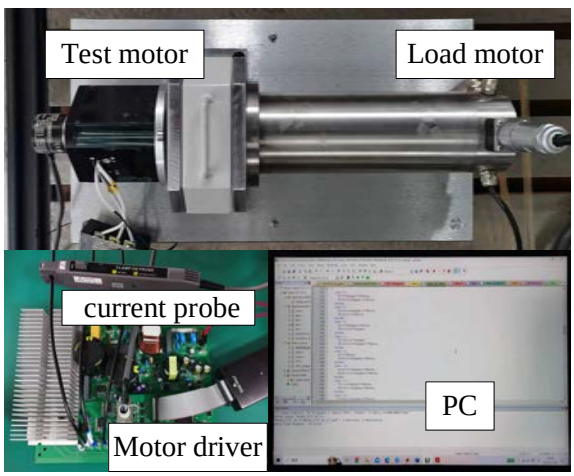

Fig. 12. Platform of experiment.

The system control block diagram is provided in Fig. 13. The parameters of the motor used in the experiments are detailed in Table I. In the experimental platform, the dead time T_d is set to 1 μs. Based on experimental measurements, the on-time delay T_{on} is approximately 0.9 μs. The oscillation time T_{set} is affected by the current variation, stray inductance, and stray resistance. Here, larger current steps and stray inductance or smaller stray resistance leads to longer T_{set}, and vice versa, making precise calculation difficult. Experimentally, its maximum value is measured as about 3.5 μs. And the A/D conversion time T_{AD} is configured as 2 μs. Based on (2), the calculated T_{min} is 7.5 μs. In hybrid PWM control, the calculation of turn-on and turn-off instants for each phase varies depending on the specific PWM method employed, making it challenging to trigger the switching devices using a unified set of microcontroller unit (MCU) timer comparison rules. To address this, the switching signals are generated by directly setting the input/output (I/O) ports to high or low levels through timer interrupt service routines. It should be noted that the execution of these routines is not instantaneous and requires a finite amount of time. To incorporate a safety margin in the experimental set up, the A/D conversion trigger is deliberately issued after a delay of at least 8 μs. Consequently, T_{min} is 10 μs in practice, with D set as 0.1. Consequently, the theoretically analyzed measurement blind zones are larger than those observed in practice. Due to the asymmetry of PWM waveform within a switching cycle, an A/D conversion strategy is employed to ensure that the sampled current value approximates the average current value over the switching cycle. When the duration time of the switching state exceeds $2T_{min}$, the A/D conversion is initiated at the midpoint of the switching state. If the duration time is less than $2T_{min}$, the A/D conversion begins 8 μs after the turn-on signal is issued.

TABLE I
PARAMETERS OF PMSM AND INVERTER

Symbol	Parameter	Value
P	Number of pole pairs	3
R	Stator resistance/Ω	0.43
L_d	d-axis inductance/mH	1.78
L_q	q-axis inductance/mH	2.49
ψ_f	Flux of permanent magnet/(V·s)	3.03×10^{-3}
J	Moment of inertia/(kg·m^2)	26×10^{-5}
V_{dc}	DC voltage/V	100
f_s	Switching frequency/kHz	10

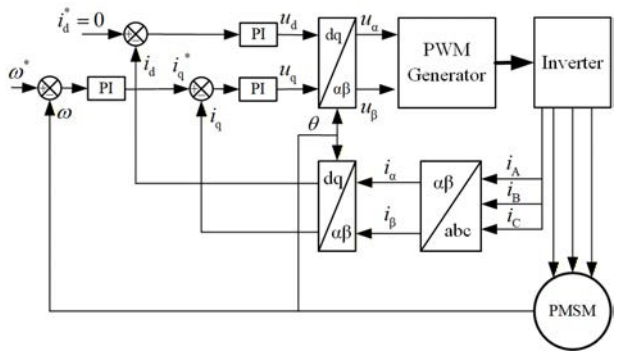

Fig. 13. Control diagram for PMSM.

In practical implementation, the DC-bus current is sampled at different switching states within one PWM period to reconstruct the phase current information. If the field-oriented control (FOC) calculation were performed only after all phase currents are reconstructed, the final sample, which may occur late in the PWM period, could leave insufficient time to complete the computation. Therefore, the currents sampled during one PWM period are used for the FOC calculations of the subsequent period, as illustrated in Fig. 14. This results in a one-PWM-period delay between the reconstructed current and the actual system current.

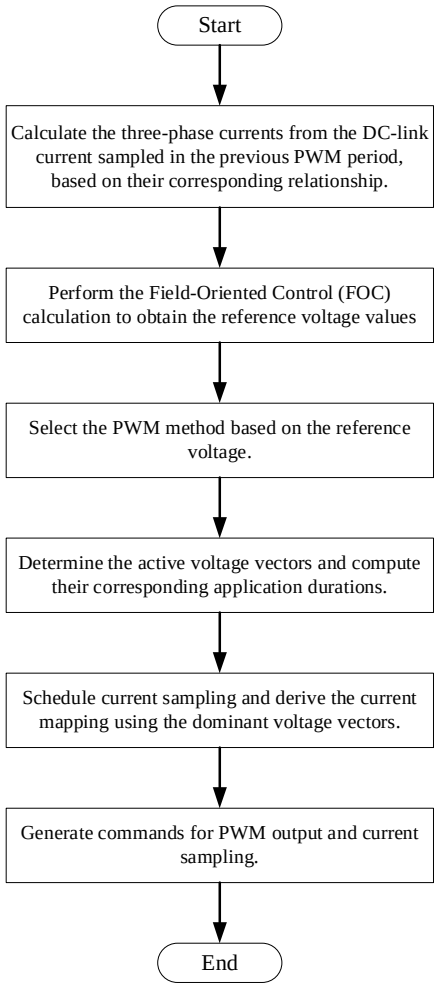

Fig. 14. Control diagram for HPWM.

The experiment was conducted in the low modulation region, where only RSPWM was used in both HPWM1 and HPWM2, with modulation ratios of 12% at 400 r/min and 19% at 800 r/min. The speed and A-phase current are shown in Figs. 15 and 16, where the blue line represents the actual current and the orange dashed line represents the reconstructed current. It can be observed that speed control was successfully achieved, and the reconstructed current closely followed the actual current.

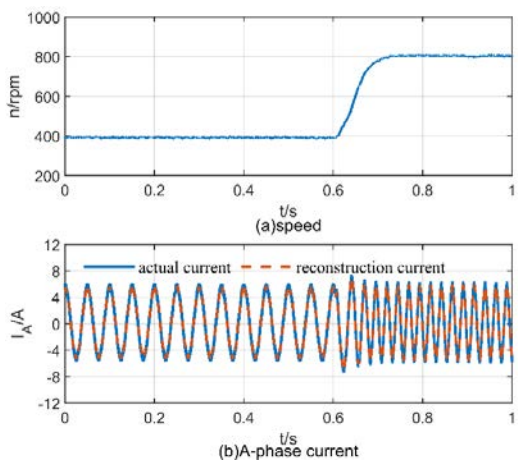

Fig. 15. Experiment result in low modulation region.

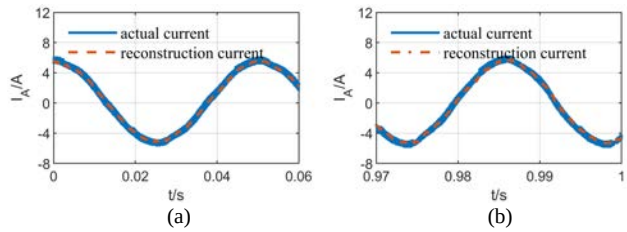

Fig. 16. A-phase current waveforms in low region (zoom in). (a) HPWM/ 400 r/min. (b) HPWM/800 r/min.

The experimental results for CMV are presented in Figs. 17 and 18. Within each switching period, the CMV remains nearly constant and exhibits six variations per electrical cycle. However, due to the dead time and propagation delays in the switching signals generated by the program, voltage spikes appear in the CMV waveform.

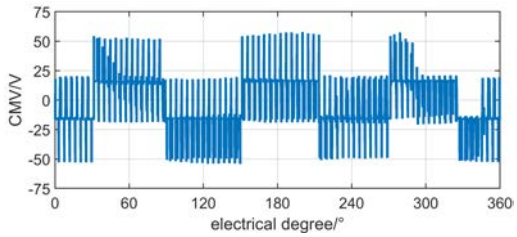

Fig. 17. Experiment result of CMV with RSPWM.

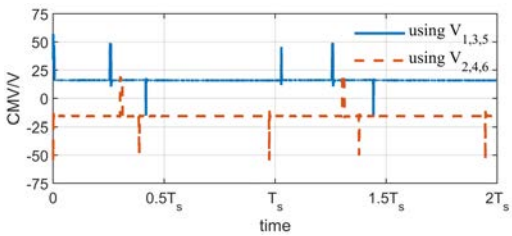

Fig. 18. Experiment result of CMV with RSPWM (zoom in).

The total harmonic distortion (THD) is used to measure the harmonic component of the current, while the standard deviation (SD) is used to measure the error between the reconstructed current and the actual current. The THD reflects the harmonic performance, with a lower value denoting fewer harmonics under the specific PWM strategy. Meanwhile, the SD is minimized precisely when the reconstructed current matches the intra-period average current. Consequently, SD directly quantifies reconstruction accuracy: minimizing SD enhances reconstruction fidelity, thereby enabling higher-precision motor control. The calculation formulas are shown in (8) and (9)

$$\mathrm{THD} = \frac{1}{I_1}\sqrt{\sum_{n=2}^{+\infty} I_n^2} \tag{8}$$

$$\mathrm{SD} = \sqrt{\frac{1}{T_\mathrm{f}}\int_0^{T_\mathrm{f}} \left(i_\mathrm{act} - i_\mathrm{rc}\right)^2 \mathrm{d}t} \tag{9}$$

where I_1 represents the root mean square (RMS) value of the fundamental component of the current; I_n represents the RMS value of the nth harmonic component; T_f is the fundamental period; i_act is the actual current; i_rc is the reconstructed current.

The THDs at 400 and 800 r/min are 9.68% and 9.25%,

respectively, while the SDs are 0.37 and 0.36A. When only RSPWM is used, there is no significant difference in SD and THD at different speeds.

Voltage-source inverters control the switching devices to generate a series of voltage pulses with equal amplitude but varying widths at their output ports. However, the desired output voltage is a continuous quantity. Thus, within a single switching period, the average value of the pulsed voltage matches the desired voltage, but the instantaneous voltage difference induces a corresponding current ripple. Consequently, harmonics and reconstruction errors are inevitably present in practical implementations. In this context, [22] derived the peak-to-peak current ripple expression for a single-phase inverter over both positive and negative half-cycles. Meanwhile, [23] analyzed the current ripple in a symmetrical three-phase inductive load by establishing Thevenin equivalent circuits for different switching states. In interior permanent magnet synchronous motor (IPMSM) drives, the three-phase inductive load varies with rotor position due to the unequal d- and q-axis inductances. Therefore, current ripple prediction is typically conducted in the dq reference frame [24].

Under the $i_d = 0$ control strategy, at full-load operation with $i_q = 6$ A, the current ripple characteristics of A-phase in the low modulation region for two different speeds are illustrated in Fig. 19. It can be observed that the current ripple exhibits only a marginal decrease as the speed increases.

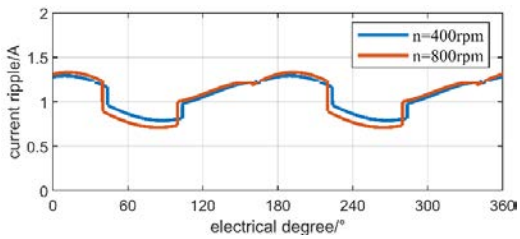

Fig. 19. Current ripple in low modulation region.

Experiments were conducted using HPWM1 and HPWM2 in the medium modulation region, where the combination of RSPWM with SVPWM was used in the HPWM1 and only RSPWM was used in the HPWM2, with modulation ratios of 23% at 1000 r/min and 50% at 2500 r/min. The experiment results are shown in Figs. 20 and 21.

The THDs at 1000 r/min are 10.73% with HPWM1 and 8.46% with HPWM2. While the SDs are 0.40 A with HPWM1 and 0.37 A with HPWM2. In this operating condition, using HPWM1 results in RSPWM control for the majority of the time, with only brief periods of SVPWM control. Therefore, there is no significant difference in SD between HPWM1 and HPWM2. However, the switching between different PWM modes results in a higher THD for HPWM1 compared to HPWM2, where only RSPWM is used. The THDs at 2500 r/min are 9.58% with HPWM1 and 8.09% with HPWM2. While the SDs are 0.43 and 0.53 A, respectively. In this operation condition, using HPWM1 results in SVPWM control for majority of the time, with only brief periods of RSPWM. Due to the involvement of zero vectors in SVPWM control, the THD in HPWM was reduced

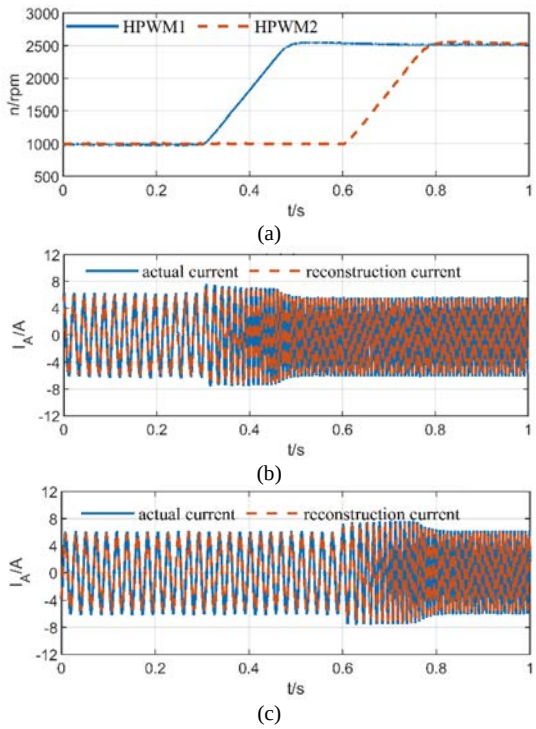

Fig. 20. Experiment result in medium modulation region. (a) speed. (b) A-phase current with HPWM1. (c) A-phase current with HPWM2.

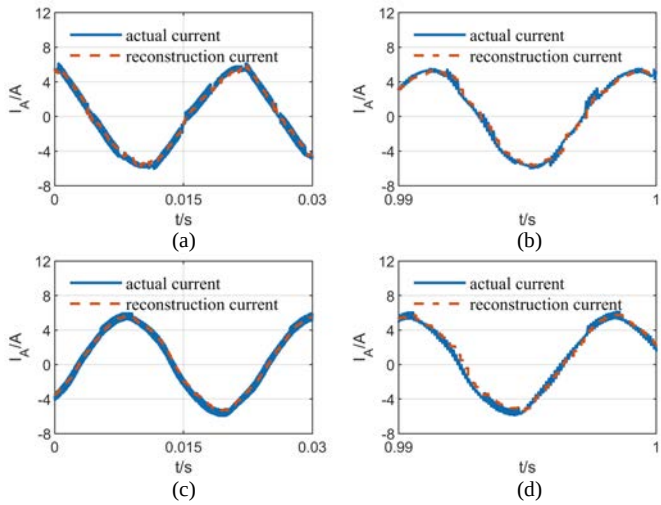

Fig. 21. A-phase current waveforms in medium modulation region (zoom in). (a) HPWM1/1000 r/min. (b) HPWM1/2500 r/min. (c) HPWM2/1000 r/min. (d) HPWM2/2500 r/min.

as voltage utilization increased, and the SD for HPWM1 was smaller than that for HPWM2.

In this operating region, HPWM1 operates as a combination of RSPWM with SVPWM, and its experimental CMV waveform is shown in Fig. 22. The RSPWM segments maintain an almost constant CMV per PWM cycle, consistent with Fig. 18, whereas the SVPWM segment, shown in Fig. 23, exhibits CMV values of $\pm V_{dc}/2$ and $\pm V_{dc}/6$, changing four times per PWM cycle. HPWM2 continues to employ only RSPWM, and its CMV waveform resembles those shown in Figs. 17 and 18.

The current ripple characteristics of the two HPWM methods in the medium modulation region at different speeds

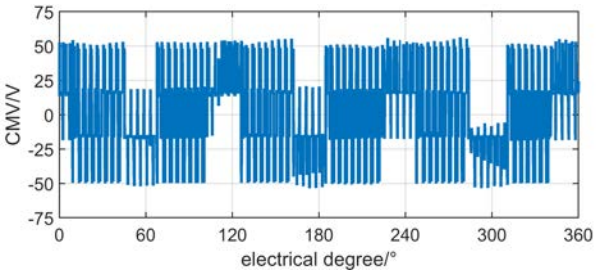

Fig. 22. Experiment result of CMV with hybrid of RSPWM and SVPWM.

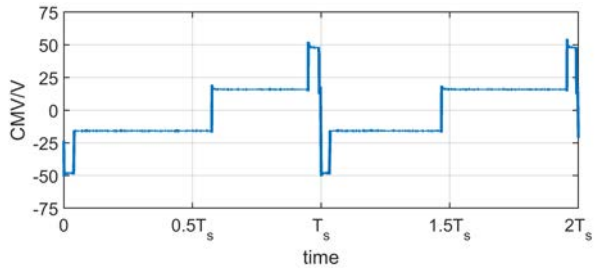

Fig. 23. Experiment result of CMV with SVPWM (zoom in).

are shown in Fig. 24. As can be observed, the current ripple of both methods decreases as the speed increases, leading to a corresponding reduction in THD. However, in practice, the reconstructed current lags the actual current by one PWM cycle due to the reconstruction process. Consequently, as the speed increases, the change in current between two consecutive PWM cycles becomes more significant, resulting in an increase in the reconstruction error.

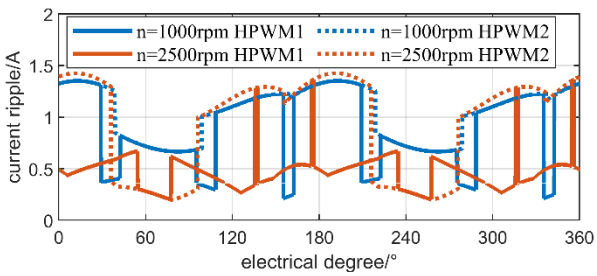

Fig. 24. Current ripple in medium modulation region.

Experiments were conducted using HPWM1 and HPWM2 in the high modulation region, where the combination of NSPWM with SVPWM was used in the HPWM1 and only NSPWM was used in the HPWM2, with modulation ratios of 68% at 3500 r/min and 96% at 5000 r/min. The experiment results are shown in Figs. 25 and 26.

The THDs at 3500 r/min are 7.77% with HPWM1 and 8.2% with HPWM2. While the SDs are 0.43 and 0.53 A, respectively. The THDs at 5000 r/min are 4.90% with HPWM1 and 4.73% with HPWM2. While the SDs are 0.63 and 0.64 A, respectively. Due to the involvement of SVPWM in HPWM1, and its duration grows with the increase in voltage utilization. As a result, the THD at 5000 r/min is lower than that at 3500 r/min, and at 3500 r/min, the THD and SD of HPWM1 are smaller than those of HPWM2. At 5000 r/min, the voltage utilization approaches 100%, resulting in the operating vectors and duration for HPWM1 and HPWM2 being similar. As a result, the THD and SD values are nearly equal.

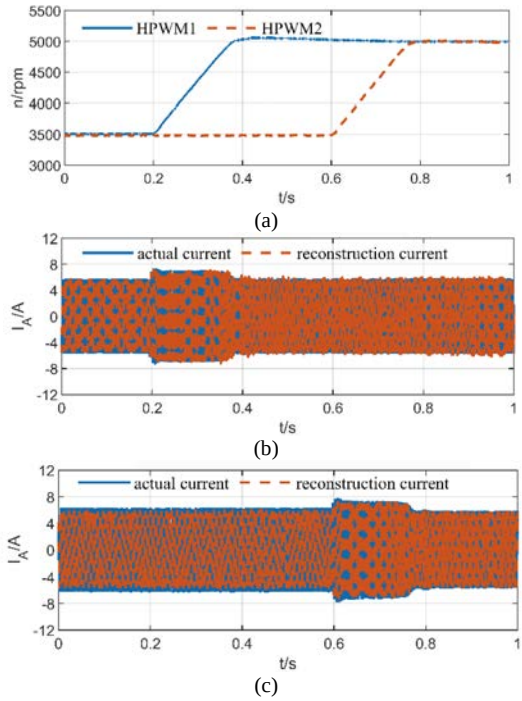

Fig. 25. Experiment result in high modulation region. (a) Speed. (b) A-phase current with HPWM1. (c) A-phase current with HPWM2.

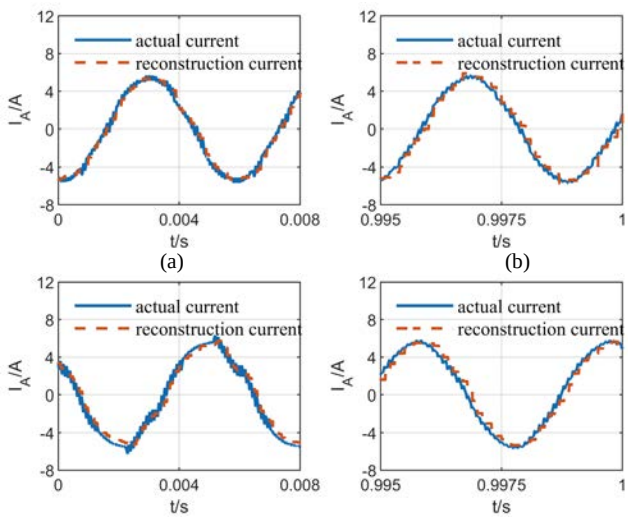

Fig. 26. A-phase current waveforms in high modulation region (zoom in). (a) HPWM1/3500 r/min. (b) HPWM1/5000 r/min. (c) HPWM2/3500 r/min. (d) HPWM2/5000 r/min.

In this operating region, HPWM1 employs the combination of NSPWM with SVPWM, with its CMV waveform shown in Fig. 27. The SVPWM segments correspond to the waveform

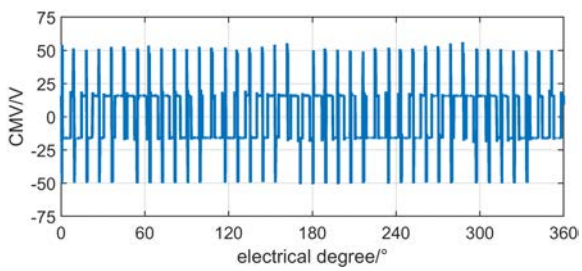

Fig. 27. Experiment result of CMV with hybrid of NSPWM and SVPWM.

in Fig. 23, whereas the NSPWM segment, shown in Fig. 28, exhibits CMV values of $\pm V_{dc}/6$, changing twice per PWM cycle. HPWM2 employs only NSPWM control, and its CMV is presented in Figs. 28 and 29. It can be observed that the CMV is primarily $\pm V_{dc}/6$ and varies twice per PWM cycle.

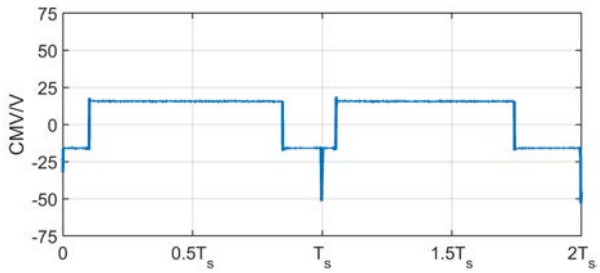

Fig. 28. Experiment result of CMV with NSPWM (zoom in).

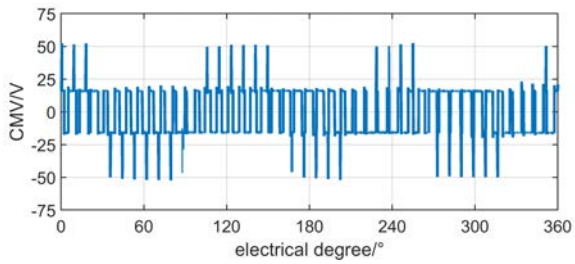

Fig. 29. Experiment result of CMV with NSPWM.

The current ripple characteristics of the two HPWM methods in the high modulation region at different speeds are shown in Fig. 30. Similarly to the behavior in the medium modulation region, the current ripple for both methods decreases with increasing speed.

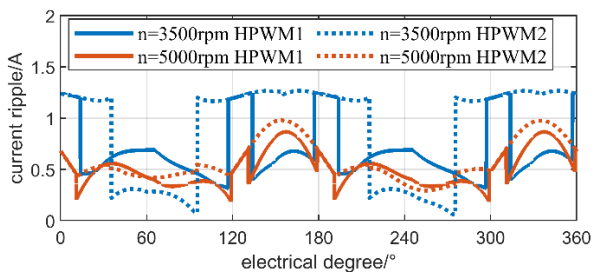

Fig. 30. Current ripple in high modulation region.

V. Algorithm for HPWM Determination

In Section IV, experiments are conducted to compare the two HPWM methods across various modulation regions, with their SD, THD, and CMV measured and evaluated. The performance is summarized in Tables II and III.

TABLE II
PERFORMANCE OF HPWM1

Speed/(r/min)	SD/A	THD	Switching loss/W (simulation)	CMV
400	0.37	9.68%	0.6831	$\pm V_{dc}/6$ Low frequency
800	0.36	9.25%	0.6841	
1000	0.40	10.73%	0.6932	$\pm V_{dc}/6$, $\pm V_{dc}/2$ High frequency
2500	0.43	9.58%	0.7115	
3500	0.45	7.77%	0.6726	$\pm V_{dc}/6$, $\pm V_{dc}/2$ High frequency
5000	0.63	4.90%	0.6848	

TABLE III
PERFORMANCE OF HPWM2

Speed/(r/min)	SD/A	THD	Switching loss/W (simulation)	CMV
400	0.37	9.68%	0.6831	$\pm V_{dc}/6$ Low frequency
800	0.36	9.25%	0.6841	
1000	0.40	8.46%	0.6882	
2500	0.43	8.09%	0.6912	
3500	0.45	8.20%	0.4142	$\pm V_{dc}/6$ Medium frequency
5000	0.63	4.73%	0.4158	

Based on the comparative results in Tables II and III:

Reconstruction accuracy: HPWM1 achieves a lower SD, indicating superior accuracy.

Harmonic performance: Both methods exhibit identical harmonic characteristics at low modulation region. HPWM2 yields lower harmonics at medium modulation region, while HPWM1 performs better at high modulation region.

Switching loss: Theoretical and simulation analyses confirm that HPWM2 has lower switching loss.

CMV performance: HPWM2 exhibits smaller amplitude and lower frequency variations, thus generating less common-mode noise and interference.

Accordingly, HPWM1 is the optimal choice when reconstruction accuracy is prioritized, whereas HPWM2 is preferable when minimizing common-mode interference and switching losses under single DC-bus current sensing.

VI. Conclusion

This paper analyzes the phase current reconstruction principle using only one DC-bus current sensor and investigates the operating regions and phase current reconstruction blind zones of SVPWM, RSPWM, and NSPWM. Two hybrid PWM methods are proposed: HPWM1, which integrates SVPWM, RSPWM, and NSPWM; and HPWM2, which combines RSPWM and NSPWM. Experimental evaluations were carried out in low, medium, and high modulation regions. On the experimental platform, both methods achieve 100% voltage utilization without current reconstruction blind zones. Based on the experimental results, the algorithm to determine the current strategy for a specific sample following HPWM1 or HPWM2 was provided.

The harmonic characteristics, reconstruction errors, and CMV of the two HPWM strategies were compared. Results show that as the voltage utilization increases, the THD decreases for both methods, while the reconstruction error increases. The THD of HPWM1 decreased from 9.68% to 4.90%, but increased to 10.73% in the transition region between RSPWM and SVPWM. Meanwhile, the SD of its reconstruction error increased from 0.37 to 0.63 A. For HPWM2, the THD decreased from 9.68% to 4.70%, while the SD of the reconstruction error increased from 0.37 to 0.64 A. Regarding CMV performance, both HPWMs share the same CMV at low modulation region, but HPWM1 shows higher CMV amplitude and frequency at medium and high modulation regions.

In the low modulation region, both HPWM methods exhibit identical performance since they operate solely with RSPWM. In the medium modulation region, HPWM1 achieves a smaller reconstruction error but exhibits increased THD due to the switching transitions between RSPWM and SVPWM. At moderately high voltage utilization levels, despite its more complex control structure, HPWM1 achieves a lower THD and reconstruction error than HPWM2 owing to the inclusion of zero vectors in SVPWM. However, at very high voltage utilization levels, particularly those approaching 100%, the performance of the two methods becomes comparable again. Under these conditions, the zero-vector duration in SVPWM becomes extremely short, and the active vector timings converge to those in NSPWM. Consequently, no significant difference is observed in harmonic performance or reconstruction error between the two strategies. In the medium and high modulation regions, HPWM1 exhibits higher CMV amplitude and frequency due to its use of SVPWM.

REFERENCES

[1] T. C. Green, and B. W. Williams, "Derivation of Motor Line-current Waveforms from the DC-link Current of an Inverter," *IEE Proceedings B (Electric Power Applications)*, vol. 136, no. 4, pp. 196–204, 1989.

[2] H. Kim, and T. M. Jahns, "Phase Current Reconstruction for AC Motor Drives Using a DC Link Single Current Sensor and Measurement Voltage Vectors," *IEEE Transactions on Power Electronics*, vol. 21, no. 5, pp. 1413–1419, Sept. 2006.

[3] J. I. Ha, "Voltage Injection Method for Three-phase Current Reconstruction in PWM Inverters Using a Single Sensor," *IEEE Transactions on Power Electronics*, vol. 24, no. 3, pp. 767–775, Mar. 2009.

[4] S. C. Yang, "Saliency-based Position Estimation of Permanent-magnet Synchronous Machines Using Square-wave Voltage Injection with a Single Current Sensor," *IEEE Transactions on Industry Applications*, vol. 51, no. 2, pp. 1561–1571, Mar.-Apr. 2015.

[5] Y. P. Shen, Z. F. Zheng, and X. L. Yang *et al*., "A Compatible SVPWM Method for DC Bus Current Sampling," *Transactions of China Electrotechnical Society*, vol. 36, no. 8, pp. 1617–1627, Apr. 2021.

[6] Y. P. Shen, K. X. Wu, and C. Z. Wu *et al*., "Complementary Non-zero Vector Current Reconstruction Strategy with Single Sensor," *Transactions of China Electrotechnical Society*, vol. 38, no. 8, pp. 2126–2135, Apr. 2023.

[7] Y. K. Gu, F. L. Ni, and D. P. Yang *et al*., "Switching-state Phase Shift Method for Three-phase-current Reconstruction with a Single DC-link Current Sensor," *IEEE Transactions on Industrial Electronics*, vol. 58, no. 11, pp. 5186–5194, Nov. 2011.

[8] H. Shin, and J. I. Ha, "Phase Current Reconstructions from DC-link Currents in Three-phase Three-level PWM Inverters," *IEEE Transactions on Power Electronics*, vol. 29, no. 2, pp. 582–593, Feb. 2014.

[9] W. C. Lee, T. J. Kweon, and D. S. Hyun *et al*., "A Novel Control of Three-phase PWM Rectifier Using Single Current Sensor," in *Proc. of 30th Annual IEEE Power Electronics Specialists Conference. Record. (Cat. No.99CH36321)*, Charleston, SC, USA, Jul. 1999, pp. 515–520.

[10] Y. K. Gu, F. L. Ni, and D. P. Yang, et al. Novel method for phase current reconstruction using a single DC-link current sensor[J]. *Electric Machines and Control*, vol. 13, no. 6, pp. 811-816, Nov. 2009.

[11] J. H. Zhu, Q. Cheng, and B. Yang, et al. Experimental research on dynamic voltage sag compensation using 2G HTS SMES[J]. *IEEE Transactions on Applied Superconductivity*, vol. 21, no. 3, pp. 2126-2130, June. 2011.

[12] B. Jung, T. Lee, and K. Nam, "Overmodulation Strategy for Inverters with a Single DC-link Current Sensor," in *Proc. of 2020 IEEE Energy Conversion Congress and Exposition (ECCE)*, Detroit, MI, USA, Oct. 2020, pp. 2649–2655.

[13] Y. P. Shen, K. X. Wu, and X. F. Yuan *et al*., "NCV-PWM Method for the Phase Current Reconstruction with DC Link Single Sensor," *IEEE Transactions on Industry Applications*, vol. 60, no. 2, pp. 3177–3187, Mar.-Apr. 2024.

[14] Y. G. Song, J. D. Lu, and Y. H. Hu *et al*., "Expanding Limit of Minimum Sampling Time Using Auxiliary Vectors for PMSM Drives with Single DC-link Current Sensor," *IEEE Transactions on Industrial Electronics*, vol. 70, no. 4, pp. 3437–3448, Apr. 2023.

[15] Y. C. Fang, B. Wang, and Y. K. Wang *et al*., "Phase Current Reconstruction Method for Permanent Magnet Synchronous Motors based on Active Zero State Pulse Width Modulation," *Transactions of China Electrotechnical Society*, vol. 40, no. 14, pp. 4483–4493, Jul. 2025.

[16] B. Saritha, and P. A. Janakiraman, "Sinusoidal Three-phase Current Reconstruction and Control Using a DC-link Current Sensor and a Curve-fitting Observer," *IEEE Transactions on Industrial Electronics*, vol. 54, no. 5, pp. 2657–2664, Oct. 2007.

[17] W. C. Lee, T. K. Lee, and D. S. Hyun, "Comparison of Single-sensor Current Control in the DC Link for Three-phase Voltage-source PWM Converters," *IEEE Transactions on Industrial Electronics*, vol. 48, no. 3, pp. 491–505, Jun. 2001.

[18] T. M. Wolbank, and P. E. Macheiner, "Current-controller with Single DC Link Current Measurement for Inverter-fed AC Machines based on an Improved Observer-structure," *IEEE Transactions on Power Electronics*, vol. 19, no. 6, pp. 1562–1567, Nov. 2004.

[19] J. Zhao, S. Nalakath, and A. Emadi, "Observer Assisted Current Reconstruction Method with Single DC-link Current Sensor for Sensorless Control of Interior Permanent Magnet Synchronous Machines," in *Proc. of IECON 2019 - 45th Annual Conference of the IEEE Industrial Electronics Society*, Lisbon, Portugal, Oct. 2019, pp. 1228–1233.

[20] F. Xiao, G. D. Xu, and C. Q. Lian *et al*., "Three-phase Current Reconstruction Strategy of Permanent Magnet Synchronous Machine Drives Using a Single Current Sensor," *Transactions of China Electrotechnical Society*, vol. 37, no. 7, pp. 1609–1617, Apr. 2022.

[21] Q. Z. Sun, and Z. F. Zhang, "Low Common-mode Voltage Model Predictive Current Control for Dual Three-phase Permanent Magnet Synchronous Motor," *Transactions of China Electrotechnical Society*, vol. 38, no. 14, pp. 3708–3722, Jul. 2023.

[22] X. L. Mao, R. Ayyanar, and H. K. Krishnamurthy, "Optimal Variable Switching Frequency Scheme for Reducing Switching Loss in Single-phase Inverters based on Time-domain Ripple Analysis," *IEEE Transactions on Power Electronics*, vol. 24, no. 4, pp. 991–1001, Apr. 2009.

[23] D. Jiang, and F. Wang, "Current-ripple Prediction for Three-phase PWM Converters," *IEEE Transactions on Industry Applications*, vol. 50, no. 1, pp. 531–538, Jan.-Feb. 2014.

[24] F. Yang, A. R. Taylor, and H. Bai *et al*., "Using *d–q* Transformation to Vary the Switching Frequency for Interior Permanent Magnet Synchronous Motor Drive Systems," *IEEE Transactions on Transportation Electrification*, vol. 1, no. 3, pp. 277–286, Oct. 2015.

Yu-Chao Fang was born in Hebei, China, in 1995. He received the B.S. degree in electrical engineering in 2017 from Tianjin University, Tianjin, China, the M.S. degree in electrical engineering in 2020 from Huazhong University of Science and Technology, Wuhan, China, and the D.Eng. in electrical engineering in 2025 from Zhejiang University, Hangzhou, China. He is currently employed at Tianjin Research Institute of Electric Science Co., Ltd. His research focuses on high-performance control of permanent magnet synchronous motors.

Yun-Chong Wang (Member, IEEE) was born in Liaoning, China, in 1987. He received the B.S. and M.S. degrees from Zhejiang University, Zhejiang, China, in 2010 and 2013, respectively, and Ph.D. degree from the Hong Kong Polytechnic University, Hong Kong, in 2017, all in electrical engineering. Since 2020, he has been an Associate Professor of Electrical Engineering with Zhejiang University. He has authored more than 30 technical papers. His research interests include the design and control of permanent magnet machines, novel electrical motors for electrical vehicles, hybrid electrical vehicles and renewable energy conversion system.

Zhang-Hao Huang (Member, IEEE) was born in Zhejiang, China, in 1997. He received the B.Eng. degree in electrical engineering from Zhejiang University, Hangzhou, China, in 2020. He is currently working toward the Ph.D. degree with the College of Electrical Engineering, Zhejiang University, Hangzhou, China. His research interests include the motion control, vibration control for flexible system and robotic actuator drive technology.

Yue-Sheng Qi (S'23) was born in Shandong, China, in 2001. He received the B.Eng. degree in electrical engineering in 2023 from Zhejiang University, Hangzhou, China, where he is currently working toward the M.S. degree in electrical engineering.

Jian-Xin Shen (M'98-SM'02) received the B.Eng. and M.Sc. degrees in electrical engineering from Xi'an Jiaotong University, Xi'an, China, in 1991 and 1994, respectively, and the Ph.D. degree in electrical engineering from Zhejiang University, Hangzhou, China, in 1997. He was with Nanyang Technological University, Singapore (1997-1999), The University of Sheffield, Sheffield, UK (1999-2002), and IMRA Europe SAS, UK. Research Centre, Brighton, U.K. (2002-2004). Since 2004, he has been a Full Professor with Zhejiang University. He has authored more than 320 technical articles, and is the inventor of more than 40 patents. His main research interests include topologies, control and applications of permanent magnet machines and drives, and renewable energies. He received 12 paper awards from IEEE and international conferences, and was granted the Nagamori Award with recognition of his contribution to permanent magnet electrical machines and high-speed electrical machines. He is a Distinguished Lecturer of IEEE IAS and VTS societies, and was the General Chair of three IEEE sponsored international conferences. More information of him can be seen at https://person.zju.edu.cn/en/jxs.